

Non-Abelian Stokes theorem and quantized Berry flux

Alexander C. Tyner¹, Shouvik Sur², Qunfei Zhou^{3,4}, Danilo Puggioni⁵,
Pierre Darancet^{4,6}, James M. Rondinelli^{1,5,6}, and Pallab Goswami^{1,2}

¹ Graduate Program in Applied Physics, Northwestern University, Evanston, Illinois, 60208, USA

² Department of Physics and Astronomy, Northwestern University, Evanston, Illinois, 60208, USA

³ Materials Research Science and Engineering Center,
Northwestern University, Evanston, IL, 60208, USA

⁴ Center for Nanoscale Materials, Argonne National Laboratory, Argonne, IL, 60439, USA

⁵ Department of Materials Science and Engineering,
Northwestern University, Evanston, Illinois, 60208, USA and

⁶ Northwestern Argonne Institute for Science and Engineering, Evanston, IL, 60208, USA

(Dated: September 30, 2022)

Band topology of anomalous quantum Hall insulators can be precisely addressed by computing Chern numbers of constituent non-degenerate bands that describe quantized, Abelian Berry flux through two-dimensional Brillouin zone. Can Chern numbers be defined for $SU(2)$ Berry connection of two-fold degenerate bands of materials preserving space-inversion (\mathcal{P}) and time-reversal (\mathcal{T}) symmetries or combined \mathcal{PT} symmetry, without detailed knowledge of underlying basis? We affirmatively answer this question by employing a non-Abelian generalization of Stokes' theorem and describe a manifestly gauge-invariant method for computing magnitudes of quantized $SU(2)$ Berry flux (spin-Chern number) from eigenvalues of Wilson loops. The power of this method is elucidated by performing N-classification of *ab initio* band structures of three-dimensional, Dirac materials. Our work outlines a unified framework for addressing first-order and higher-order topology of insulators and semimetals, without relying on detailed symmetry data.

I. INTRODUCTION

Niu1985, The basic concepts of topological band theory were developed by considering global properties of non-degenerate energy bands of time-reversal symmetry breaking, two-dimensional insulators¹⁻⁹. The band eigenfunctions of such systems are determined up to arbitrary complex phase factors, i.e. $\psi_n(\mathbf{k})$ and $e^{i\alpha_n(\mathbf{k})}\psi_n(\mathbf{k})$ are equally good candidate eigenfunctions for the n -th band, with $n = 1, 2, 3, \dots, N$. This $U(1)$ redundancy for individual bands leads to Abelian Berry's connection, $\mathbf{A}_n(\mathbf{k}) = -i \langle \psi_n | \nabla | \psi_n \rangle$ and corresponding Berry's curvature $\mathbf{\Omega}_n(\mathbf{k}) = \nabla \times \mathbf{A}_n(\mathbf{k})$. By integrating $\mathbf{\Omega}_n^j$ over the two-dimensional Brillouin zone (BZ), one arrives at the quantized flux of $U(1)$ curvature, $\int d^2k \mathbf{\Omega}_n(\mathbf{k}) = 2\pi C_n$, where C_n is the Chern number of band n . There exist many reliable methods for computing C_n . For example, by measuring the Berry's phase accrued by $\psi_n(\mathbf{k})$ when it is parallel transported along any non-intersecting closed contour and relating it to enclosed flux by Stokes theorem.

Can quantized flux exist for two-fold degenerate bands of parity+time-reversal (\mathcal{PT}) invariant systems? The two-fold degeneracy gives rise to local $SU(2)$ redundancy of each band; as $\{\psi_{n,\uparrow}(\mathbf{k}), \psi_{n,\downarrow}(\mathbf{k})\}^T$, $g_n(\mathbf{k})\{\psi_{n,\uparrow}(\mathbf{k}), \psi_{n,\downarrow}(\mathbf{k})\}^T$ are equally good candidate wavefunctions. The curvature, $F_{n,s,s'}$, of $SU(2)$ Berry's connections, $\mathbf{A}_{n,s,s'}(\mathbf{k}) = -i \langle \psi_{n,s}(\mathbf{k}) | \nabla | \psi_{n,s}(\mathbf{k}) \rangle$, is gauge covariant. Therefore, there are many conceptual

subtleties in assigning gauge-invariant non-Abelian Berry's flux. If global symmetries such as $U(1)$ spin-conservation⁶ or mirror symmetry¹⁰ are present, it becomes possible to assign a global spin quantization axis, ($U(1)$ gauge-fixing) of $SU(2)$ connections. In the case of a mirror symmetry, one can separate the eigenspace into two subspaces, labeled by the eigenvalues of the mirror operator, and calculate C_n in each subspace. In the absence of mirror symmetry there is currently no suitable, gauge-invariant method, for computation of flux. Topological classification of general \mathcal{PT} symmetric, two-dimensional insulators, preserving \mathcal{P} and \mathcal{T} individually, thus relies on assignment of the Fu-Kane Z_2 index⁷. Furthermore, generic two dimensional planes, embedded in a three-dimensional system, need not support their own time-reversal invariant momenta (TRIM) points, precluding assignment of even the Z_2 index. Nevertheless, many such planes have been proposed as forms of higher-order topological insulators¹¹⁻¹⁴. *Does assignment of flux in a Kramers degenerate band structure require mirror symmetry? Does a Z_2 index imply the presence of an underlying quantized flux?* In this work we answer these questions utilizing the method of Wilson loops (WLs), demonstrating that quantized flux can be computed for any n -fold rotationally symmetric plane through analysis of the non-Abelian Berry's gauge connections^{15,16}. This method is shown to be applicable in both tight-binding models as well as *ab initio* data.

Consider a closed, non-intersecting path lying in the xy plane and respecting the m -fold symmetry of

the plane. The WL of $SU(2)$ connections of n -th Kramers-degenerate bands along this contour, parameterized by $\mathbf{k}(l)$, is defined as

$$W_n = P \exp \left[i \oint \sum_{j=1}^2 A_{j,n}(\mathbf{k}(l)) \frac{dk_j}{dl} dl \right], \quad (1)$$

$$= \exp \left[i \theta_n(k_0) \hat{\Omega}_n(k_0) \cdot \boldsymbol{\sigma} \right], \quad (2)$$

where P denotes path ordering and k_0 corresponds to the edge size of the loop. The intra-band connections of n -th band, are defined according to the formula $A_{j,n,s,s'}(\mathbf{k}) = -i\psi_{n,s}^\dagger(\mathbf{k})\partial_j\psi_{n,s'}(\mathbf{k})$, where $\psi_{n,s}(\mathbf{k})$ are the eigenfunctions of n -th band, with $s = \pm 1$ denoting the Kramers index, and $\partial_j = \frac{\partial}{\partial k_j}$. The gauge invariant angle $\theta_n(k_0)$ can be related to the magnitude of non-Abelian, Berry's flux by employing a non-Abelian generalization of Stokes's theorem^{17–20}. The gauge dependent, three-component, unit vector $\hat{\Omega}_n(k_0)$ defining the orientations in $SU(2)$ color space will not be used for computing any physical properties. When the n -th Kramers-degenerate bands support quantized flux of magnitude $|2M\pi|$ with $M \in \mathbb{Z}$, $|\Delta\theta_n(k_0)| = |\theta_n(k_0) - \theta_n(0)|$ will interpolate from 0 to $|2M\pi|$ as k_0 is systematically increased from 0 to a final value k_f , when the area enclosed by the loop becomes equal to the area of two-dimensional BZ. Such quantized flux can be found for two-dimensional planes preserving \mathcal{P} symmetry, as well as planes supporting a global $U(1)$ symmetry. In other cases, such as generic two-dimensional insulators which break \mathcal{P} and \mathcal{T} symmetries, but for which the product \mathcal{PT} is preserved, it is possible for non-Abelian flux through the full zone to be non-quantized. This absent quantization in the non-Abelian phase measured by WL in the first BZ indicates the presence of a twisted boundary condition. As will be shown, twisted boundary conditions do not exclude assignment of quantized flux in the extended BZ.

The current standard for topological analysis of *ab initio* data, involves calculation of Wannier charge centers (WCCs). WCCs, the gauge invariant spectra of straight Wilson loops, also known as Polyakov loops (PL)¹⁵ have emerged as powerful tools for describing topology of quasi-particle band-structures^{21–24}. Generally PLs are used for diagnosis of the Fu-Kane strong and weak Z_2 indices and, in the presence of mirror-symmetry or non-degenerate bands, are utilized to determine quantized Berry's flux²⁵. However, in the absence of mirror-symmetry PLs fail to recognize flux in \mathcal{PT} symmetric band structures. Further, PLs are known to fail in identifying non-trivial topology for the class of higher-order topological insulators (HOTIs). The necessity of the proposed method can be summarized by Fig.

(1), detailing the symmetry requirements to assign a two-dimensional bulk invariant based on quantized Berry's flux to a Kramers degenerate band using current methods. The shortfalls of these methods are clear as, in the absence of mirror or $U(1)$ spin conservation symmetry, no existing method can capture the bulk invariant. As a result a large number of systems, particularly those with even integer bulk invariants invisible to the Z_2 index, have gone undetected.

We will explicitly demonstrate the power of this method by performing topological classification of *ab initio* band structures of Dirac semimetals (DSMs). We choose to examine DSMs as the generic two-dimensional planes lying between the Dirac nodes and perpendicular to the axis of nodal separation have been identified as examples of two-dimensional higher-order topological insulators with gapped edge states, while the high-symmetry planes are identified by either a Z_2 index, or a mirror Chern number, depending on the presence of mirror symmetry^{11,12,14}. DSMs thus offer the chance to study distinct types of higher order- and first order- topological insulators, embedded in a single material.

Na_3Bi was proposed as the first candidate material for realizing stable DSMs, which arise from linear touching between a pair of two-fold, Kramers-degenerate bands at isolated points of momentum space, along an axis of n -fold rotation (say the \hat{z} or c -axis)²⁶. The Dirac points are simultaneously protected by the combination of parity and time-reversal symmetries (\mathcal{PT}) and the n -fold rotational (\mathcal{C}_n) symmetry^{27,28}. The low energy Hamiltonian is written as, $H(\mathbf{k}) = \epsilon_0(\mathbf{k})\mathbb{1} + \sum_{j=1}^5 d_j(\mathbf{k})\Gamma_j$, where Γ_j 's are again five, mutually anti-commuting, 4×4 matrices, and $\mathbb{1}$ is the 4×4 identity matrix²⁶. The topological properties of conduction and valence bands are controlled by the $O(5)$ vector field $d_1 = Ak_x$, $d_2 = Ak_y$, $d_3 = Bk_z(k_x^2 - k_y^2)$, $d_4 = 2Bk_xk_yk_z$, and $d_5 = M_0 - M_1k_z^2 - M_2(k_x^2 + k_y^2)$, where A , B , M_0 , M_1 , and M_2 are band parameters. For Na_3Bi , the parameters $M_0 < 0$, $M_1 < 0$, and $M_2 < 0$ capture band inversion effects, leading to two Dirac points along the six-fold, screw axis at $(0, 0, \pm k_D)$, with $k_D = \sqrt{M_0/M_1}$. The particle-hole anisotropy term $\epsilon_0(\mathbf{k})$ does not affect band topology.

For describing low-energy physics of massless Dirac fermions, d_3 and d_4 terms can be ignored in the renormalization group sense^{26,29,30}. Such approximate theories predict topologically protected, loci of zero-energy surface-states, also known as the *helical Fermi arcs*, joining the projections of bulk Dirac points on the (100) and the (010) surface- Brillouin zones. Therefore, the spectroscopic detection of *helical Fermi arcs* was often considered to be the smoking gun evidence of bulk topology of DSMs. How-

ever, these terms cannot be ignored for addressing topological properties of generic planes and they are responsible for gapping out the helical edge states for all $|k_z| < k_D$ and $k_z \neq 0$ ³¹⁻³³, and giving rise to higher-order topology^{13,14}.

II. AB INITIO BAND STRUCTURES

The crystal structure of Na₃Bi, belongs to the space group P6₃/mmc and has the lattice constants $a = b = 5.49$ Å, $c = 9.78$ Å. It consists of two non-equivalent Na sites, denoted by Na(1) and Na(2). The honeycomb layers formed by Na(1) and Bi are stacked along the c-axis, with Na(2) sites located between the layers. For computational details please see the supplementary materials. The calculated band structures within the energy window -3 eV and $+2$ eV are displayed in Fig. 2(a). We have labeled the Kramers-degenerate bands, according to their energy eigenvalues at the Γ point, with $E_n(0) < E_{n+1}(0)$. The bulk Dirac points arise from linear touching between bands $n = 6$ and $n = 7$, along the six-fold, screw axis ($A - \Gamma - A$ line or the k_z axis) at $(0, 0, \pm k_D)$, with $k_D \approx \pm 0.29 \times \frac{\pi}{c}$. Their reference energy coincides with the Fermi level.

A. Bulk Topology

In order to perform topological analysis of various bands, we have employed maximally localized Wannier functions calculated using the WANNIER90 package³⁴. We will calculate WLs of individual $SU(2)$ Berry's connections of bands $n = 1$ through $n = 6$ by utilizing the Z2Pack software package^{23,25}. In calculating WLs, we have followed the hexagonal path $abcdef$, shown in Fig. 2(b).

We first focus on the results of the WL for occupied bands in the $k_z = 0$ mirror plane. In this plane, we find that the Dirac band ($n = 6$) as well as four remote bands ($n = 1, 2, 3, 5$) support non-zero flux of varying magnitude (see Fig. 2(d)) for which quantization occurs for a contour exactly enclosing the two-dimensional BZ. Due to the presence of mirror symmetry, flux could also have been computed via WCCs, yielding identical results. By contrast, away from the mirror planes, WCCs can no longer be utilized to determine flux. For more details of WCCs in these planes please see the supplementary materials. Computing WLs for the occupied Dirac band at generic topologically non-trivial planes defined by $|k_z| < k_D$, $|\Delta\theta_6(k_0)|$ shows 0 to 2π interpolation for a contour enclosing an area slightly greater than the two-dimensional BZ. This behavior is in accordance with the low energy lattice model of Na₃Bi

presented in the supplementary information. For $|k_z| > k_D$, $|\Delta\theta_6(k_0)|$ does not exhibit such interpolation, indicating that these planes are topologically trivial. These topological properties of Dirac bands are identical to what have been found from the effective, four-band model of sp -hybridized DSMs²⁰.

While topological diagnosis of the high-symmetry planes of Na₃Bi benefits from the presence of mirror symmetry, one can also consider a DSM where the high-symmetry plane lying perpendicular to the direction of nodal separation lacks mirror symmetry. One such system is β -CuI, which was proposed as a DSM by Le et. al³³, with the Dirac nodes lying along the k_z axis. For full computational details of this material please consult the supplementary materials. As β -CuI belongs to space group $R\bar{3}m$, the high-symmetry xy planes support three-fold rotational symmetry. Mirror symmetry is therefore absent and the current topological classification of the planes is limited to assignment of a Z_2 index. In Fig. 3(b), we show that for the high-symmetry and generic planes lying between the Dirac nodes, the method of WLs can be utilized to identify a quantized flux. These results emphasize the presence of flux as the common topological invariant of two-dimensional topological insulators, regardless of the underlying symmetry.

B. Conclusions

Recently, Tyner et. al²⁰ demonstrated that unlike Weyl semimetals, Dirac semimetals do not support Fermi arcs, loci of two, degenerate zero energy state beginning and terminating at the projection of the bulk nodes²⁰. Rather, a generic plane lying between the Dirac nodes supporting a non-zero relative Chern number supports two, non-degenerate gapped surface states. Only at the high-symmetry mirror planes can we locate gapless points on the surface with the number of gapless points being determined by the magnitude of the mirror Chern number. Using the iterative Greens function method³⁵ and the Wannier Tools software package³⁶, we plot the spectral density on the (100) surface of Na₃Bi in Fig. 4). These results verify that at a generic value of $|k_z| < k_D$, the (100) surface of Na₃Bi supports gapped surface states. Only at the $k_z = 0$ mirror plane do we find a gapless state in correspondence with the admission of mirror Chern number $|\mathcal{C}_m| = 1$, by this plane.

In recent works, the bulk-boundary correspondence of two dimensional higher order insulators has been characterized by the presence of corner localized states in those corners of a two-dimensional slab that align with the corners of the primitive two-

dimensional unit cell^{11,12,14}. Fixing $|k_z| < k_D$, and performing an exact diagonalization calculation for a slab consisting of 10×10 primitive unit cells in the xy plane, we schematically depict the wavefunction localization of the four corner-localized states present at half filling in Fig. (4(b)). The localization pattern of these states captures the bulk-boundary correspondence and verifies the HOTI classification of the xy planes between the Dirac nodes. However, we emphasize that these states are not mid-gap states, well separated from the bulk states¹⁴, posing a significant challenge for experimental detection and re-enforcing the need for a robust method of bulk classification.

In summary, we have proposed a method capable of quantifying non-Abelian flux through any plane regardless of underlying crystal symmetries. We have successfully applied this method to *ab initio* data of multiple Dirac materials. Our results are insensitive to the number of underlying bands, suggesting the topology of real materials can be comprehensively addressed with stable, bulk invariants.

ACKNOWLEDGMENTS

A. C. T., S. S., Q. Z., P. D. and P. G. were supported by the National Science Foundation MRSEC program (DMR-1720139) at the Materials Research Center of Northwestern University. D.P. and J.M.R. acknowledge the Army Research Office under Grant No. W911NF-15-1-0017 for financial support and the DOD-HPCMP for computational resources. Use of the Center for Nanoscale Materials (CNM), an Office of Science user facility, was supported by the U.S. Department of Energy, Office of Science, Office of Basic Energy Sciences, under Contract No. DE-AC02-06CH11357.

Appendix A: In-plane Wilson Loop

For concreteness, let us consider the Hamiltonian $H = \sum_{\mathbf{k}} \Psi^\dagger(\mathbf{k}) \hat{H}(\mathbf{k}) \Psi(\mathbf{k})$, where $\Psi(\mathbf{k})$ is a four-component spinor, and the Bloch Hamiltonian operator can be written as

$$\hat{H}(\mathbf{k}) = N_0(\mathbf{k}) \mathbb{1} + \sum_{j=1}^5 N_j(\mathbf{k}) \Gamma_j, \quad (\text{A1})$$

where the $O(5)$ vector field $\mathbf{N}(\mathbf{k})$ encodes details of band-structures, and Γ_j 's are five, mutually anti-commuting, 4×4 matrices, such that $\{\Gamma_i, \Gamma_j\} = 2\delta_{ij}$. Specifically we set, $\Gamma_{i=1,2,3} = \tau_i \otimes \sigma_1$, $\Gamma_4 = \tau_2 \otimes \sigma_0$, $\Gamma_5 = \tau_3 \otimes \sigma_0$, where τ_0 and σ_0 are two 2×2 identity matrices. The two sets of Pauli matrices

τ_j and σ_j with $j = 1, 2, 3$ operate on the spin and orbital degrees of freedom respectively. For clarity, we consider

$$\mathbf{N}(\mathbf{k}) = [t_p \sin k_x, t_p \sin k_y, t_d \sin k_z (\cos k_x - \cos k_y), t_d \sin k_z \sin k_x \sin k_y, t_s (\Delta - \cos k_x - \cos k_y - \cos k_z)], \quad (\text{A2})$$

which describes \mathcal{C}_4 -symmetric DSMs. Here, t_s, t_p, t_d are independent hopping functions. The dimensionless parameter Δ controls topological phase transitions. In particular, when $1 < \Delta < 3$, all five components of $\mathbf{N}(\mathbf{k})$ vanish at the Dirac points, located at $\mathbf{k} = (0, 0, \pm k_{D,1})$ with $\cos k_{D,1} = (\Delta - 2)$.

It is convenient to compute WL by following a \mathcal{C}_4 symmetric path, denoted $ABCD$. An image of this path is available in the supplementary information. Without any loss of generality we will choose the point A with $(k_x, k_y) = (-k_0, -k_0)$ as our reference point. When the Kramers-degenerate wave functions are parallel transported between an initial point \mathbf{k}_i and a final point \mathbf{k}_f , the matrix-valued, non-Abelian Berry's phase^{15,37,38} is described by the Wilson line (or non-Abelian holonomy)

$$W_{i,f} = P \exp[i \int_{l_i}^{l_f} \sum_{j=1}^2 a_j(\mathbf{k}(l)) \frac{dk_j}{dl} dl], \quad (\text{A3})$$

where P denotes path ordering, and we choose to work with the gauge choice,

$$a_j(\mathbf{k}) = \frac{1}{2|\mathbf{N}|(|\mathbf{N}| + N_5)} [(N_1 \partial_j N_2 - N_2 \partial_j N_1) \Gamma_{12} + (N_2 \partial_j N_3 - N_3 \partial_j N_2) \Gamma_{23} + (N_3 \partial_j N_1 - N_1 \partial_j N_3) \Gamma_{31} + \sum_{a=1}^3 (N_a \partial_j N_4 - N_4 \partial_j N_a) \Gamma_{a4}], \quad (\text{A4})$$

where $\Gamma_{ij} = [\Gamma_i, \Gamma_j]/(2i)$. We note that $a_j(\mathbf{k})$ is singular at TRIM locations in which $N_5 = -|\mathbf{N}|$ as discussed in Tyner et. al²⁰. We have parameterized the line, joining two points as $k_j(l)$, $\mathbf{k}_i = \mathbf{k}(l_i)$ and $\mathbf{k}_f = \mathbf{k}(l_f)$. Therefore, the WL for path $ABCD$ can be obtained as the ordered product of four straight Wilson lines as

$$W_{ABCD}(k_0) = W_{A,B} W_{B,C} W_{C,D} W_{D,A}. \quad (\text{A5})$$

Since $W_{ABCD}(k_0) \in Spin(4)$, we can parametrize it as

$$W_{ABCD}(k_0) = W_{ABCD,c}(k_0) W_{ABCD,v}(k_0) = \begin{bmatrix} \exp[i\theta_c(k_0) \hat{\mathbf{n}}_{c_j}(k_0) \cdot \boldsymbol{\sigma}] & 0 \\ 0 & \exp[i\theta_v(k_0) \hat{\mathbf{n}}_v(k_0) \cdot \boldsymbol{\sigma}] \end{bmatrix}. \quad (\text{A6})$$

Here, $W_{ABCD,c}(k_0) \in SU(2)$ and $W_{ABCD,v}(k_0) \in SU(2)$ are the WLs for the respective $SU(2)$ connections of conduction and valence bands. Two angles $\theta_c(k_0)$ and $\theta_v(k_0)$ are gauge-invariant and two

$O(3)$ unit vectors $\hat{\mathbf{n}}_c(k_0)$ and $\hat{\mathbf{n}}_v(k_0)$ define gauge-dependent orientations in color space.

If we wish to abstain from making a gauge choice and compute WLs in a purely numerical fashion, the straight Wilson line along \hat{j} for band n can be rewritten as^{11,21,24},

$$W_j(\mathbf{k}) = F_{j,\mathbf{k}+N_j\Delta k_j} \dots F_{j,\mathbf{k}+\Delta k_j} F_{j,\mathbf{k}}, \quad (\text{A7})$$

where $F_{j,\mathbf{k}+N_j\Delta k_j} = \langle u_{\mathbf{k}+N_j\Delta k_j}^n | u_{\mathbf{k}}^n \rangle$, $\Delta k_j = 2\pi/N_j$, and $|u_{\mathbf{k}}^n\rangle$ is the Bloch function of band n at \mathbf{k} .

From $\theta_{c/v}(k_0)$ we can construct other gauge-invariant quantities, such as the eigenvalues of WLs $\exp[\pm i\theta_{c/v}(k_0)]$, the trace of WLs $\text{Tr}[W_{ABCD,c/v}](k_0) = 2\cos[\theta_{c/v}(k_0)]$, and the Vandermonde determinant $D_V[W_{ABCD,c/v}](k_0) = 2i\sin[\theta_{c/v}(k_0)]$. In gauge theory literature, $\text{Tr}[W_C]$ is the most widely studied observable. It is useful for detecting interpolation of W_C between the center elements $\pm\sigma_0$ of $SU(2)$ group, leading to $\text{Tr}[W_C] = \pm 2$. When $\theta_{c,v} = 2l\pi$ [$(2l+1)\pi$], with $l \in \mathbb{Z}$, $W_{C,c/v} = \sigma_0$ [$-\sigma_0$]. We determine both $\text{Tr}[W_{ABCD,c/v}]$ and $D_V[W_{ABCD,c/v}]$ to find $\theta_{c/v}$.

For Abelian connections of non-degenerate bands, the Stokes's theorem directly relates θ_c and θ_v to the underlying Berry's flux. In the non-degenerate case, as k_0 is tuned from 0 to π , $\theta_{c/v}(k_0)$ can interpolate between 0 and $2l\pi$, $l \in \mathbb{Z}$. The Chern number is precisely given by $\theta_{c/v}(k_0 = \pi)$. The windings of θ_c and θ_v for the non-Abelian connections also indicate the presence of chromo-magnetic flux, and non-trivial second homotopy classification. However, the interpretation of flux requires a non-Abelian generalization of Stokes's theorem^{17-19,39-41}, and $\theta_{c,v}$ can be related to the surface-ordered, integrals of parallel-transported, non-Abelian curvatures

$$W_{xy} = P_s \exp \left[i \int d^2k W_{A,O}^\dagger(k_x, k_y) f_{xy}(k_x, k_y) W_{A,O}(k_x, k_y) \right], \quad (\text{A8})$$

where, P_s denotes surface ordering, and $f_{xy}(k_x, k_y) = \partial_x a_y - \partial_y a_x + i[a_x, a_y]$ corresponds to covariant curvatures. Here, $W_{A,O}(k_x, k_y)$ is the parallel transport operator, defined in Eq. (A3), whose initial and final points are respectively located at $\mathbf{k} = (-k_0, -k_0)$ and $\mathbf{k} = (k_x, k_y)$, shown schematically in Fig. (5(c)).

For the model given by eq. (A2), all topologically non-trivial, xy planes with $|k_z| < k_D$, $\theta_c(k_0)$ and $\theta_v(k_0)$ display non-trivial windings, as the size of loop $ABCD$ is systematically increased. For the parameters chosen, ($t_p/t_s = 0.75$ and $t_d/t_s = 0.5$), convergence to the quantized result is found for a contour only slightly larger than the entire two-dimensional, BZ torus. This causes W_{ABCD} to interpolate between \mathbb{Z}_2 centers of the respective $SU(2)$

subgroups. For some intermediate value of $0 < k_0 < \pi$, $\theta_{c/v}$ reaches π . Topologically trivial planes do not show such interpolations. On the other hand, generic planes lying between quadratically dispersing Dirac nodes display 0 to 4π windings. Since this method does not require any detailed knowledge of the underlying basis, it can be efficiently used for diagnosing bulk topology from *ab initio* band-structures. In contrast to the Abelian projections²⁰, this method can only detect the absolute magnitude of flux.

1. Analytical results

In the above description of the Wilson loop and in the low-energy derivation presented in the subsequent section, identification of quantized flux relies on tracking interpolation of the WL between $SU(2)$ center elements $\pm\sigma_0$. A continuous interpolation between these elements is taken to be in correspondence with the interpolation of the non-Abelian flux, $\theta_{c/v}$, by 2π as $\text{Tr}W_{xy} = 2\cos\theta_{c/v}$. Here we provide proof of the correspondence between non-Abelian loop and quantized non-Abelian flux. To do so, we consider the model,

$$H(\mathbf{k}) = \sin\alpha(k_\perp) \cos(m\phi)\Gamma_1 + \sin\alpha(k_\perp) \sin(m\phi)\Gamma_2 + \cos\alpha(k_\perp)\Gamma_3 \quad (\text{A9})$$

where Γ_i 's are defined previously and $\cos\alpha(k_\perp) = (\Lambda - k_\perp^{2m})/(\Lambda + k_\perp^{2m})$, with Λ defining the skyrmion core size. This model is chosen to prove correspondence with non-Abelian flux as all WLs are analytically tractable. When $\text{sgn}(\Lambda) > (<)0$, this model is in a topological (trivial) phase for which it is known to support quantized $|2m\pi|$ (0) Berry's flux⁶. However, in the current basis, this model is block off-diagonal, and the $SU(2)$ intra-band Berry's gauge connections are matrix valued, i.e. non-Abelian. In order to prove that the non-Abelian Wilson loop precisely measures flux, we consider a path enclosing a sector of the circular Brillouin zone with central angle $2\pi/N$. The non-Abelian WL can thus be written as,

$$W_N = W_{k_\perp, k_\perp=0}^{k_\perp=\infty}(\phi = \phi_i) W_{\phi, \phi_i}^{\phi_i+2\pi/N}(k_\perp=\infty) W_{k_\perp, k_\perp=\infty}^{k_\perp=0}(\phi = \phi_i + 2\pi/N). \quad (\text{A10})$$

After some algebra, using the definition for the intra-band Berry's gauge connections written previously, we arrive at the form,

$$\frac{1}{2} \text{Tr}[W_N] = \cos^2\Omega + \cos(2m\pi/N) \sin^2\Omega, \quad (\text{A11})$$

where,

$$\Omega = \begin{cases} \pi/2, \text{sgn}(\Lambda) > 0 \\ 0, \text{sgn}(\Lambda) < 0 \end{cases}. \quad (\text{A12})$$

Therefore we can conclude that in the topological phase, $\text{sgn}(\Lambda) > 0$, $\text{Tr}W_N/2 = \cos(2m\pi/N)$. As such we have directly shown correspondence between quantized Berry's flux, $\theta_{c/v}$ and the WL, validating the above procedure of tracking $SU(2)$ center elements.

Additionally, we could consider analyzing $W_\phi(\mathbf{k}_\perp)$ as a function of k_\perp . After some algebra, we arrive at the expression,

$$\text{Tr}W_\phi(\mathbf{k}_\perp)/2 = \cos(m\pi) \cos(m\pi\sqrt{10 - 6\cos(2\alpha)}/2). \quad (\text{A13})$$

We note that in the simple case, $m = 1$, $\text{Tr}W_\phi(\mathbf{k}_\perp)/2 = -1$ along the curve defining band inversion, namely $k_\perp^{2m} = \Lambda$. However, such correspondence vanishes for $m > 1$, as $W_\phi(\mathbf{k}_\perp) = \pm\sigma_0$ at general values of k_\perp , which are not in correspondence with the location of band inversion.

In order to analytically demonstrate the effectiveness of WLs in detecting the presence of quantized non-Abelian flux for five-component models, such as those describing higher-order insulators, we consider the following continuum version of (A1),

$$\begin{aligned} \hat{H}(\mathbf{k}) &= \sum_{j=1}^5 N_j(\mathbf{k})\Gamma_j = B_1 k_\perp (\cos\phi\Gamma_1 + \sin\phi\Gamma_2) \\ &+ B_2(k_z)k_\perp^2 (\cos 2\phi\Gamma_3 + \sin 2\phi\Gamma_4) + N_5(k_\perp, k_z)\Gamma_5, \end{aligned} \quad (\text{A14})$$

where $(k_x, k_y) = k_\perp(\cos\phi, \sin\phi)$. We define $N_5(k_\perp, k_z)$, such that for $k_\perp = 0(\infty)$, $|k_z| < k_D$, $N_5/N = -(+)1$ while for $k_\perp = 0(\infty)$, $|k_z| > k_D$, $N_5/N = +(+)1$. The non-Abelian gauge connection, A_ϕ , can then be calculated following eq. (A4). The Wilson loop follows as,

$$W_\phi^\pm(k_\perp, k_z) = \mathcal{P}\exp\left[i\int_0^{2\pi} A_\phi(\mathbf{k})d\phi\right], \quad (\text{A15})$$

where (\pm) indicates the Kramers degenerate conduction and valence bands respectively. Defining $W_\phi^\pm(k_\perp, k_z) = \exp(i\Phi^\pm \cdot \sigma)$, we examine the gauge invariant quantity $\cos\Phi^\pm = -\cos\alpha^\pm$. This quantity is equivalent to $\text{Tr}(W_\phi^\pm)/2$. Solving for α^\pm , we arrive at the form,

$$\begin{aligned} \alpha^\pm &= \pi \left[\left(\frac{(B_1^2 \pm 2B_2(k_z)^2 k_\perp^2) k_\perp^2}{\mathbf{N}(\mathbf{N} + N_5)} - 1 \mp 2 \right)^2 \right. \\ &\left. + \frac{B_1^2 B_2(k_z)^2 k_\perp^6}{\mathbf{N}^2(\mathbf{N} + N_5)^2} \right]^{\frac{1}{2}}. \end{aligned} \quad (\text{A16})$$

We will now investigate this quantity in three important limits (1) at the nodal plane, (2) at the mirror plane, and (3) at a generic plane.

Nodal Plane: At the nodal plane, $|k_z| = k_D$, as $k_\perp \rightarrow 0$, \mathbf{N} scales as k_\perp . As a result $\alpha^\pm(k_\perp \rightarrow 0) = 2\pi$ while in the limit $k_\perp \rightarrow \infty$, $\alpha^\pm(k_\perp \rightarrow \infty) = \pi|-1 \mp 2|$. We therefore find the quantized flux in the nodal plane to be $|\Delta\Phi| = |\Phi(k_\perp = \infty) - \Phi(k_\perp = 0)| = \pi$, the critical value.

Mirror Plane: For the current model, $B_2(k_z) = k_z B_2$, therefore at the mirror plane, $k_z = 0$, we set $B_2(k_z) = 0$. In order for a plane to support quantized non-Abelian flux of magnitude 2π , we must be able to show that $\text{Tr}W_\phi^\pm$ evolves adiabatically from $+2 \rightarrow +2$, through $\text{Tr}W_\phi^\pm = -2$. Similar to the calculation of WCCs, this adiabatic evolution must be treated carefully as it is possible to have a plane in which $|\Delta\Phi|$ exceeds π as a function of k_\perp before returning to zero. When analyzing $\text{Tr}W_\phi^\pm$, this manifests as two locations of k_\perp at which $\text{Tr}W_\phi^\pm = -2$ without reaching $\text{Tr}W_\phi^\pm = +2$ at an intermediate value. We note $\alpha^\pm(k_\perp \rightarrow 0, \infty) = \pi|-1 \mp 2|$, while the values of k_\perp for which $\text{Tr}W_\phi^\pm = -2$ at the mirror plane are found by solving,

$$\left| \frac{B_1^2 k_\perp^2}{\mathbf{N}(\mathbf{N} + N_5)} - 1 \mp 2 \right| = 2n, n \in \mathcal{N}. \quad (\text{A17})$$

This is satisfied if there exists a value of k_\perp where $N_5 = 0$, thus the mirror plane supports quantized non-Abelian flux of magnitude 2π .

Generic Plane: At a generic value of k_z , we can again conclude that $\alpha^\pm(k_\perp \rightarrow 0, \infty) = \pi|-1 \mp 2|$, however we can no longer analytically determine how α^\pm interpolates between these values. We thus solve numerically, fixing $B_2(k_z) = k_z B_2$ and $N_5 = (B_3 k_\perp^4 + B_4 k_z^2 - \Delta)$. This process indicates that only planes for which $|k_z| < k_D$ support quantized non-Abelian flux of magnitude 2π .

2. Minimal tight binding models

To demonstrate the necessity of the proposed in-plane Wilson loop method, consider the tight-binding model, $H(\mathbf{k})_n = \sum_{j=1}^5 N_j^n(\mathbf{k})\Gamma_j$, where,

$$\begin{aligned} \mathbf{N}(\mathbf{k})^n &= \{t_p \sin k_x, t_p \sin k_y, t_d \sin k_x \sin k_y, \lambda_n(\mathbf{k}), \\ &t_s(3/2 - \cos k_x - \cos k_y)\}. \end{aligned} \quad (\text{A18})$$

The lattice constants have been set to unity, t_j 's are hopping parameters with units of energy, and Γ_j 's are five, mutually anti-commuting, 4×4 matrices, such that $\{\Gamma_i, \Gamma_j\} = 2\delta_{ij}$. Specifically we set, $\Gamma_{i=1,2,3} = \tau_i \otimes \sigma_1$, $\Gamma_4 = \tau_2 \otimes \sigma_0$, $\Gamma_5 = \tau_3 \otimes \sigma_0$, where $\sigma_{i=1,2,3}(\tau_{i=1,2,3})$ τ_0 and σ_0 are the Pauli matrices

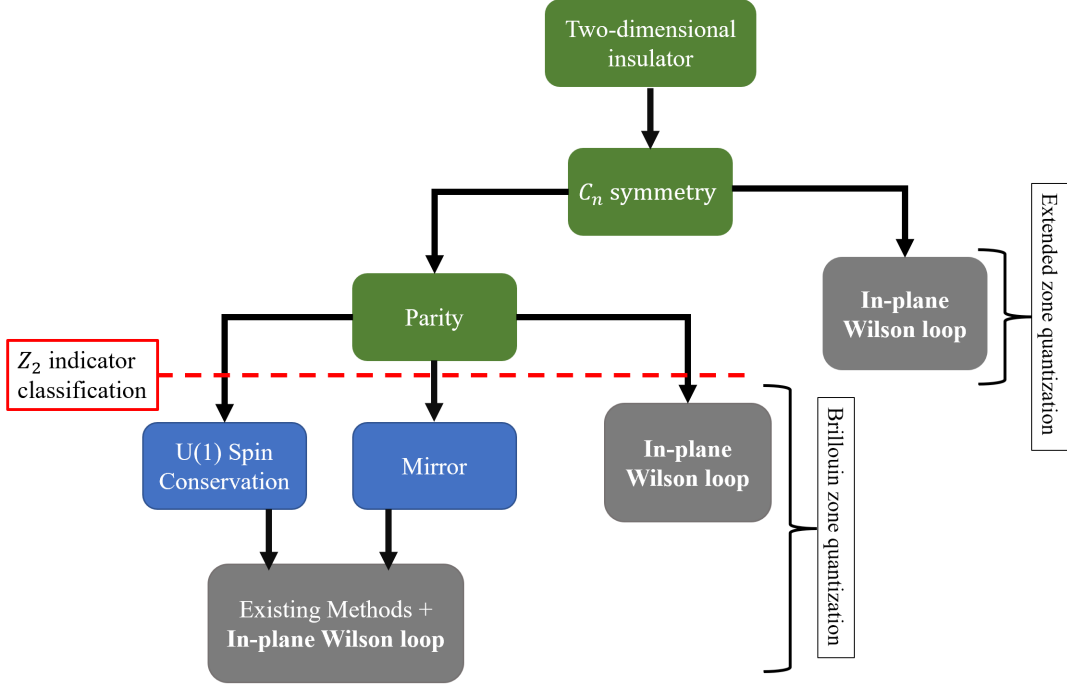


FIG. 1. Guide for assignment of bulk invariant based on magnitude of quantized Berry's flux for two-dimensional insulators. All crystalline insulators support C_n symmetry. If parity symmetry is additionally present the Fu-Kane \mathbb{Z}_2 index can be assigned; however this index can not detail the magnitude of the bulk invariant and does not capture systems supporting an even integer bulk invariant. If in addition to parity, mirror or $U(1)$ spin conservation symmetries are present, there are existing methods for obtaining the bulk invariant. However, we emphasize that these symmetries are not common in nature, particularly when considering two dimensional planes, embedded in three dimensions. Nevertheless, the in-plane Wilson loop is capable of capturing quantized flux in each case. If only C_n symmetry is present, an extended zone scheme is required.

and two 2×2 identity matrices respectively. We then define $\lambda_n(\mathbf{k}) = t_d(\cos(nk_x) - \cos(nk_y))$. Parity symmetry is given by $\mathcal{P} = \tau_3 \otimes \sigma_3$, such that $\mathcal{P}^\dagger H(\mathbf{k})\mathcal{P} = H(-\mathbf{k})$. Despite the presence of parity symmetry, assignment of a Fu Kane strong TI index is inconclusive. This is clearly seen in the case $n = 2$; at the TRIM locations only $N_5(\mathbf{k}) \neq 0$, thus \mathcal{P} and $H(\mathbf{k})_n$ are both diagonal. The constituent states of each Kramers pair are thus labeled by opposite eigenvalues of \mathcal{P} at each TRIM location. If we were to rely on the WCC spectra for diagnosis of bulk topology, eigenvalues of $\text{Im}(\text{Ln}(W_x(k_y)))/(2\pi)$ denoted $\bar{x}(k_y)$, we would conclude that the model is trivial, see Fig. (5(b)). It is only by computing the WL following the path ABCD shown in Fig. (5(c)), with results shown in Fig. (5(d)), that it is clear this model supports Berry's flux, for which quantization to $|2\pi|$ is commensurate with the BZ when $n = 2$. If $n = 1$, multiple components of $\mathbf{N}(\mathbf{k})$ survive at the TRIM locations obscuring winding of the five component vector field. This is the reason a WL along the boundary of the BZ is not quantized. The non-Abelian phase is exhibiting a twisted boundary

condition. However, by expanding the area enclosed by the WL contour, a full winding from $0 \rightarrow 2\pi$ can again be identified. Furthermore, a corresponding quantized flux in the BZ can be identified for arbitrary n via Abelian gauge fixing with respect to the rotation generator Γ_{12} , as detailed in Tyner et. al²⁰. Nevertheless, WL has the advantage of being a basis-agnostic method which can be readily applied to *ab initio* data using existing software.

3. Higher winding numbers

It is possible to construct a tight-binding model exhibiting quantized non-Abelian flux greater than 2π . As an example, we consider the Bloch Hamiltonian, $H(\mathbf{k}) = \sum_{j=1}^5 N_j(\mathbf{k})\Gamma_j$, where,

$$\mathbf{N}(\mathbf{k}) = \{\lambda_1^1(\mathbf{k}), \lambda_2^1(\mathbf{k}), \lambda_1^2(\mathbf{k}), \lambda_2^2(\mathbf{k}), t_s(3/2 - \cos k_x - \cos k_y)\}, \quad (\text{A19})$$

defining $\lambda_n^1 = t_{d,n} \sin(nk_x) \sin(nk_y)$ and $\lambda_n^2 = t_{d,n}(\cos(nk_x) - \cos(nk_y))$. We will work with $t_{d,1} =$

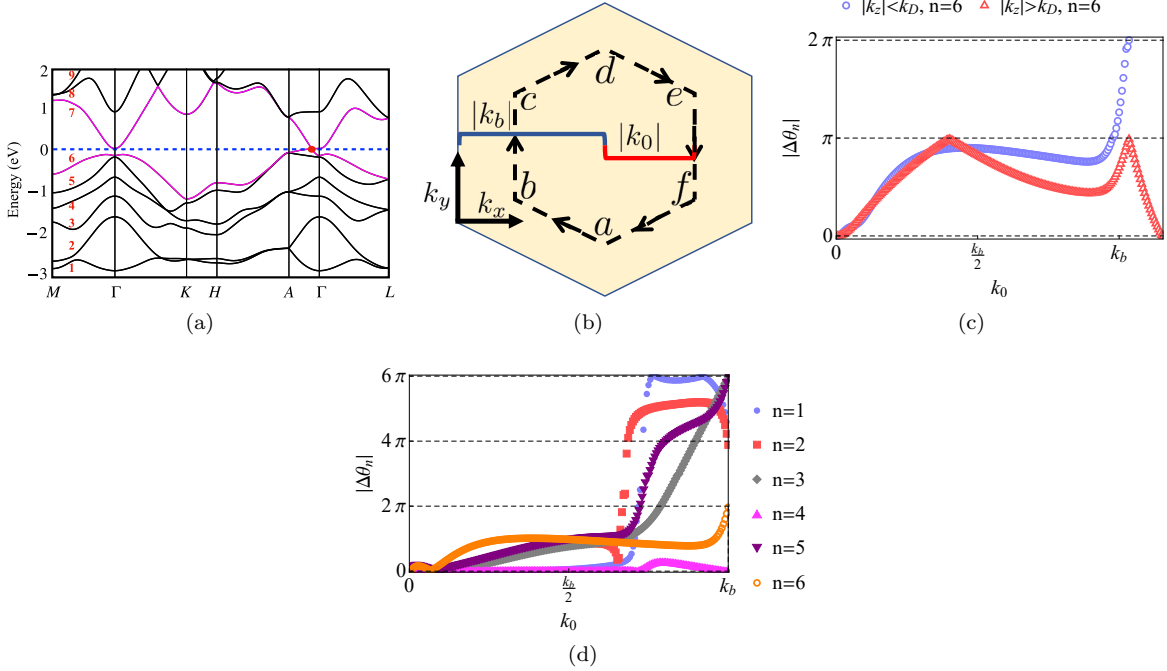


FIG. 2. (a) The *ab initio* band structures of Na₃Bi are plotted along various high-symmetry directions, and the Kramers-degenerate bands are labeled, following an ascending order of energy eigenvalues at the Γ point. The linear touching between bands $n = 6$ and $n = 7$ (purple colored), along the six-fold, screw axis $\Gamma - A$, gives rise to bulk Dirac points (red dot), lying at the Fermi level (dashed line). (b) The Wilson loops are calculated following the hexagonal loop $abcdef$. We increase k_0 from zero to $k_b = \pi/a$, when the enclosed area becomes equal to that of hexagonal Brillouin zone (yellow). The gauge invariant eigenvalues of Wilson loops are given by $e^{\pm i\theta_n(k_0)}$, where n is the band index. For topologically non-trivial bands, supporting non-Abelian flux of magnitude $2M\pi$, $|\Delta\theta_n| = |\theta_n(k_0) - \theta_n(0)|$ will interpolate from 0 to $2M\pi$, as k_0 is increased from 0 to $k_b + \epsilon$, where $\epsilon \geq 0$. (c) For all xy planes, lying between (outside) two Dirac points, the occupied Dirac band, $n = 6$, is non-trivial (trivial). (d) At the $k_z = 0$ mirror plane, the remote bands $n = 1, 2(n = 3, 5)$ also support quantized flux of magnitude $4\pi(6\pi)$, demonstrating that the WL method can capture arbitrary flux strength. For more details of higher-winding please consult the supplementary information.

$t_{d,2} = t_s$. For this model, parity symmetry is generated by the identity matrix, precluding assignment of a Fu-Kane Z_2 index. Calculating WCCs, $\bar{x}(k_y)$, we find the result shown in Fig. (6(a)), indicating a trivial configuration. This result is in-line with the absence of gapless edge states as shown in Fig. (6(b)). When applying open boundary conditions in two-dimensions, we note the existence of mid-gap corner states, shown in Fig. (6(d)) and (6(e)). However, the nested Wilson loop calculations yields trivial results in this model. As such, we are left without a method capable of diagnosing topology under periodic boundary conditions.

Implementing the WL, we find the results shown in Fig. (6(c)). These results demonstrate beautiful quantization of non-Abelian flux within the Brillouin zone to a magnitude of $|4\pi|$.

Contrast to nested Wilson loops: The method of nested Wilson loops (NWLs)^{11,12} has been developed to identify higher-order topological insulators.

More precisely, the method of NWLs is used to identify bulk-boundary correspondence for hinge/corner localized states when edge states are gapped. Application of this method to the tight-binding model given by eq. (A18) in the main-body, yields a non-trivial result when all hopping parameters are non-zero. As this model supports mid-gap corner states, the NWL can be used to describe the bulk boundary correspondence of these states. NWLs will fail when $t_d = 0$ as gapless edge states are present. WL does not suffer from this dependence on edge/corner states and can be applied successfully for arbitrary hopping parameters. More importantly, in the model given by eq. (A19), both WCCs and NWL fail to indicate non-trivial topology despite the presence of mid-gap corner states. This leaves the question of bulk-boundary correspondence an open one under the current paradigm of topological classification. Only WL is capable of yielding information of non-trivial topology under periodic

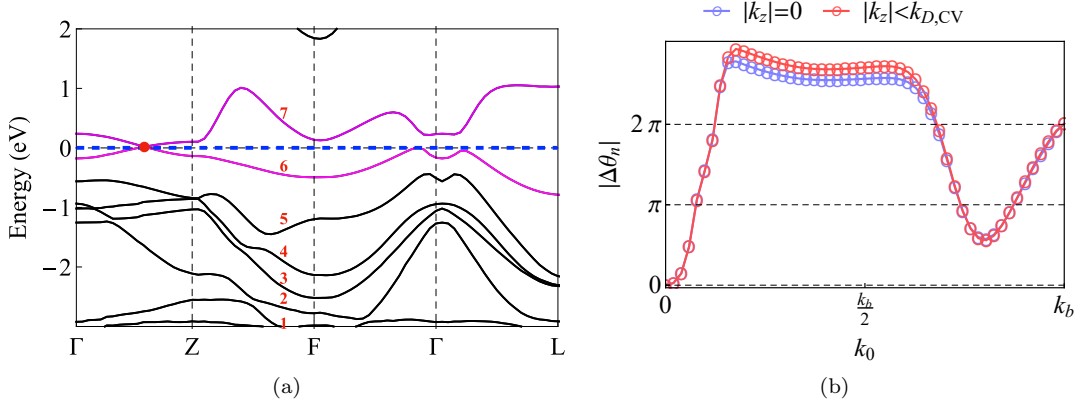


FIG. 3. (a) Band structure of β -CuI in the primitive unit cell along high symmetry path detailed by Le et. al.³³. Kramers pairs which touch at the Fermi energy at $\mathbf{k} = (0, 0, \pm k_D)$ to produce Dirac point (bands in Dirac subspace) are colored purple. Dirac point is noted with red dot. (b) Results of Wilson loop calculation at high-symmetry plane, $k_z = 0$, and generic value of $|k_z| < k_{D,CV}$, where $k_{D,CV}$ is the location of the Dirac point in the conventional unit cell for the occupied Dirac band, $n = 6$. Wilson loop is calculated as a function of the area enclosed by the Wilson loop path. This calculation indicates that band 6 supports non-Abelian flux of magnitude 2π for all planes such that $|k_z| < k_{D,CV}$.

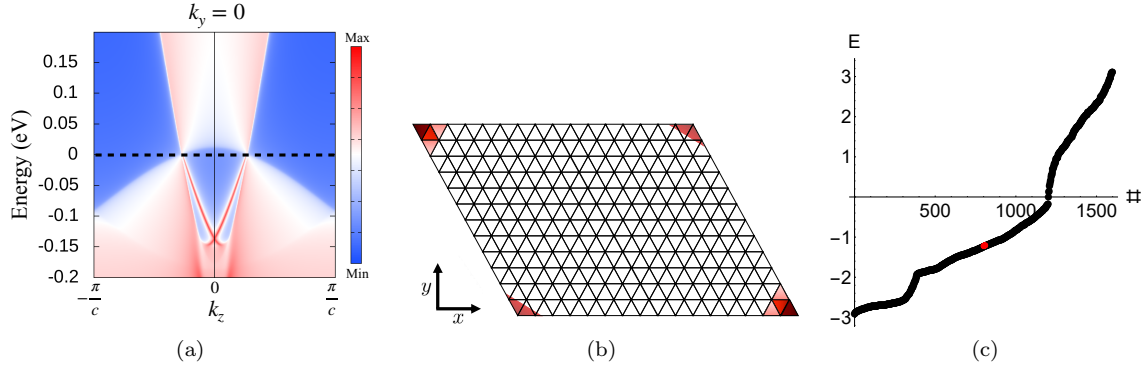


FIG. 4. (a) The (100) edge state dispersion for Na_3Bi along the k_z axis shows the dependence of gap as a function k_z . The normalizability of surface-states breaks down at the images of bulk Dirac points on the surface Brillouin zone. The existence (non-existence) of gapped, surface-states for higher-order topological insulators (trivial insulators) can only be justified by computing quantized, Berry's flux. (b) Schematic of localization pattern for the four corner-localized states at half-filling in eight band tight binding model of Na_3Bi , setting $|k_z| < |k_D|$ and solving on a finite slab of 10×10 primitive unit cells. Darker shading corresponds to stronger localization. The localization pattern confirms that the xy planes between the Dirac nodes, which have been identified as higher order topological insulators, support corner localized states. (c) States resulting from exact diagonalization calculation. Localization shown in (b) corresponds to states colored in red. We note that while these states exist at half-filling, they do not fall at zero energy and are not separated in energy from the bulk states.

boundary conditions, emphasizing non-Abelian flux as the universal signature of non-trivial topology under periodic boundary conditions.

Appendix B: $C_{n=3,6}$ symmetric tight-binding models

In order to demonstrate how implementation of WL can be extended from the four-fold rotationally symmetric system, to a three- and six-fold system, in a controlled manner, we introduce two tight binding Hamiltonians of two Kramers degenerate bands. The first is a two-dimensional topological insula-

tor with six-fold rotational symmetry, described by the Hamiltonian, $H = \sum_{\mathbf{k}} \Psi^\dagger(\mathbf{k}) \hat{H}(\mathbf{k}) \Psi(\mathbf{k})$, where $\Psi(\mathbf{k})$ is a four-component spinor. The Bloch Hamiltonian operator is written as $\hat{H}(\mathbf{k}) = \sum_{j=1}^5 N_j(\mathbf{k}) \Gamma_j$, where the five component vector $\mathbf{N}(\mathbf{k})$ contains details of the band structure and the Γ matrices have been previously defined. We will consider,

$$\mathbf{N}(\mathbf{k}) = t\{(2 \sin(k_1 + k_2) + \sin k_1 + \sin k_2)/3, (\sin k_1 - \sin k_2)/\sqrt{3}, 4(\cos k_1 + \cos k_2 - 2 \cos(k_1 + k_2))/3, 4(\cos k_2 - \cos k_1)/\sqrt{3}, \Delta - (\cos(k_1 + k_2) + \cos k_1 + \cos k_2)\}, \quad (\text{B1})$$

where t is a hopping parameter with units of energy that will be fixed such that $t = 1$ in all calculations, and $k_j = \mathbf{k} \cdot \mathbf{a}_j$, for lattice vectors, $\mathbf{a}_1 = a(\sqrt{3}, 1)/2$, $\mathbf{a}_2 = a(-\sqrt{3}, 1)/2$. We have set $a = 1$ such that there exists unit lattice spacing in all directions.

Upon fixing $\Delta = 2$, we compute the WL, following the closed, directed path shown in Fig. (2(b)), with the results displayed in Fig. (7(a)). This procedure is then repeated fixing $\Delta = 4$, indicating that for $\Delta = 2(4)$ the model is in a topological (trivial) phase supporting quantized flux of magnitude $|2\pi|(0)$.

Next, we turn to a three-fold symmetric example, altering $\mathbf{N}(\mathbf{k})$ in eq. (B1), to the form,

$$\mathbf{N}(\mathbf{k}) = t\{\sin k_1, -\sin k_2, -\sin(k_1 - k_2), 0, (\Delta + \cos k_1 + \cos k_2 + \cos(k_1 + k_2))\}, \quad (\text{B2})$$

where t is again a hopping parameter with units of energy, fixed to unity, and $k_j = \mathbf{k} \cdot \mathbf{a}_j$, for lattice vectors, $\mathbf{a}_1 = a(\sqrt{3}, 1)/\sqrt{6}$, $\mathbf{a}_2 = a(\sqrt{3}, -1)/\sqrt{6}$. The three-fold environment is particularly important to examine as three-fold planes do not support mirror symmetry when embedded in a three-dimensional structure. Thus, although parity symmetry is given by $\mathcal{P} = \Gamma_5$, and Z_2 invariant $\nu_0 = +1$ can be assigned, such systems have escaped classification via quantized flux. WLs are calculated following the same procedure defined previously, with the results shown in Fig. (7(b)). These results demonstrate that when $\Delta = 2(4)$ the model is in a topological (trivial) phase, supporting flux $|2\pi|(0)$.

Appendix C: Details of Na₃Bi analysis

All first-principles calculations based on the density-functional theory are performed using the Vienna *ab initio* simulation package^{42,43}, and the exchange-correlation potentials use the Perdew-Burke-Ernzerhof (PBE) parametrization of the generalized gradient approximation⁴⁴. An $11 \times 11 \times 7$ grid of \mathbf{k} points and a plane-wave cutoff energy

520 eV are used for self-consistent field calculations. All calculations incorporate the effects of spin-orbit coupling. The qualitative features of DSM phase of Na₃Bi have been well characterized with the first principles calculations of band structures and various spectroscopic, and transport measurements^{26,45–49}.

When performing a topological analysis of Dirac and Weyl semimetals, it is common to calculate the WCCs of all occupied states, we present such an analysis in Fig. (8). At the high-symmetry planes the behavior of WCCs can be used to determine the strong TI invariant as well as the mirror Chern number^{50–63}, however, as shown in the main body, there are instances where this correspondence breaks down. Further, only by performing a WL can one obtain topological information at a generic plane. It is also common to search for helical Fermi arcs as a signature of the bulk topology, examining the surface spectral density at a fixed energy as a function of momenta, as seen in Fig. (10). Our results demonstrate that such depictions of the surface modes can lead to the misconception that genuine helical Fermi arcs are present in a Dirac semimetal. We thus emphasize the importance of bulk topological classification using WLs. This method can be used for establishing the topological universality class of DSMs in various compounds such as Cd₃As₂⁶⁴, BiAuBi-family⁶⁵, Cu₃PdN⁶⁶, LiGaGe-family⁶⁷, PdTe₂⁶⁸, β' -PtO₂^{14,69}, VAl₃⁷⁰, β -CuI³³, KMgBi^{14,71}, FeSn⁷².

Appendix D: Details of β -CuI analysis

β -CuI belongs to space group $R\bar{3}m$ and was recently proposed as a type-I Dirac semimetal³³. The bulk DPs fall along the k_z axis, and are thus protected by the three-fold rotational symmetry of the k_z axis as well as \mathcal{PT} symmetry. First-principles calculations are carried out using the same packages implemented for Na₃Bi. The BZ is sampled with an $8 \times 8 \times 8$ grid of \mathbf{k} points and a plane-wave cutoff of 500 eV is used for self-consistent field calculations. The calculated band structures within the energy window $-3eV$ and $2eV$ is displayed in Fig. (3(a)) with the Kramers-degenerate bands labeled according to their energy at the Γ point, with $E_n(0) < E_{n+1}(0)$. *Bulk-edge correspondence:* In Le et. al³³, it was shown that β -CuI does not support Fermi arcs, but rather gapped edge states for all generic planes satisfying $|k_z| < k_D$ when open-boundary conditions are applied perpendicular to the direction of nodal separation. We can thus conclude that the bulk-edge correspondence of these states is given by the presence of quantized non-Abelian flux.

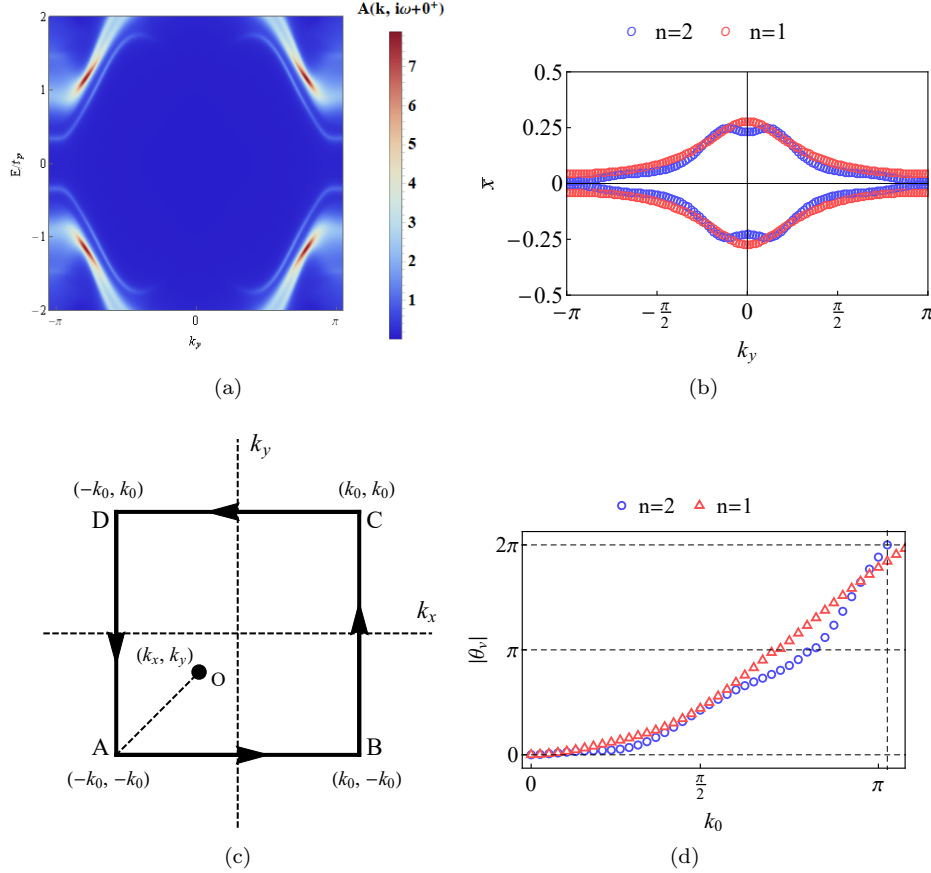


FIG. 5. (a) Spectral density on (10) edge for tight-binding model given by eq. (A18) fixing $n = 2$ in arbitrary units. The edge states are gapped when setting $t_{p,1} = t_{p,2} = t_s = t_d = 1$, and considering a semi-infinite slab along the x direction with periodic boundary conditions along k_y . (b) Wannier center charges (WCCs), $\bar{x}(k_y)$, fixing $n = 1, 2$ for identical choice of hopping parameters. The WCC spectra does not display winding in either case, indicating trivial topology. (c) The C_4 -symmetric path $ABCD$ for computing Wilson loops. (d) Results of WL following a C_4 symmetric closed contour. As the area enclosed by the contour approaches the area of the Brillouin zone ($k_0 = \pi$), the flux converges to $|2\pi|$ for $n = 2$, while a contour slightly larger than the area of the zone must be used when $n = 1$, capturing the non-trivial topology.

- ¹ D. J. Thouless, M. Kohmoto, M. P. Nightingale, and M. den Nijs, “Quantized Hall conductance in a two-dimensional periodic potential,” *Phys. Rev. Lett.* **49**, 405–408 (1982).
- ² F. D. M. Haldane, “Model for a quantum Hall effect without Landau levels: condensed-matter realization of the parity anomaly,” *Phys. Rev. Lett.* **61**, 2015–2018 (1988).
- ³ Qian Niu, D. J. Thouless, and Yong-Shi Wu, “Quantized Hall conductance as a topological invariant,” *Phys. Rev. B* **31**, 3372–3377 (1985).
- ⁴ C. L. Kane and E. J. Mele, “ Z_2 topological order and the quantum spin hall effect,” *Phys. Rev. Lett.* **95**, 146802 (2005).
- ⁵ T. Fukui, Y. Hatsugai, and H. Suzuki, “Chern numbers in discretized Brillouin zone: Efficient method of

computing (spin) Hall conductances,” *J. Phys. Soc. Jpn* **74**, 1674–1677 (2005).

- ⁶ B Andrei Bernevig, Taylor L Hughes, and Shou-Cheng Zhang, “Quantum spin hall effect and topological phase transition in hgte quantum wells,” *Science* **314**, 1757–1761 (2006).
- ⁷ Liang Fu and C. L. Kane, “Topological insulators with inversion symmetry,” *Phys. Rev. B* **76**, 045302 (2007).
- ⁸ Liang Fu, C. L. Kane, and E. J. Mele, “Topological insulators in three dimensions,” *Phys. Rev. Lett.* **98**, 106803 (2007).
- ⁹ J. E. Moore and L. Balents, “Topological invariants of time-reversal-invariant band structures,” *Phys. Rev. B* **75**, 121306 (2007).
- ¹⁰ Jeffrey C. Y. Teo, Liang Fu, and C. L. Kane, “Surface states and topological invariants in three-

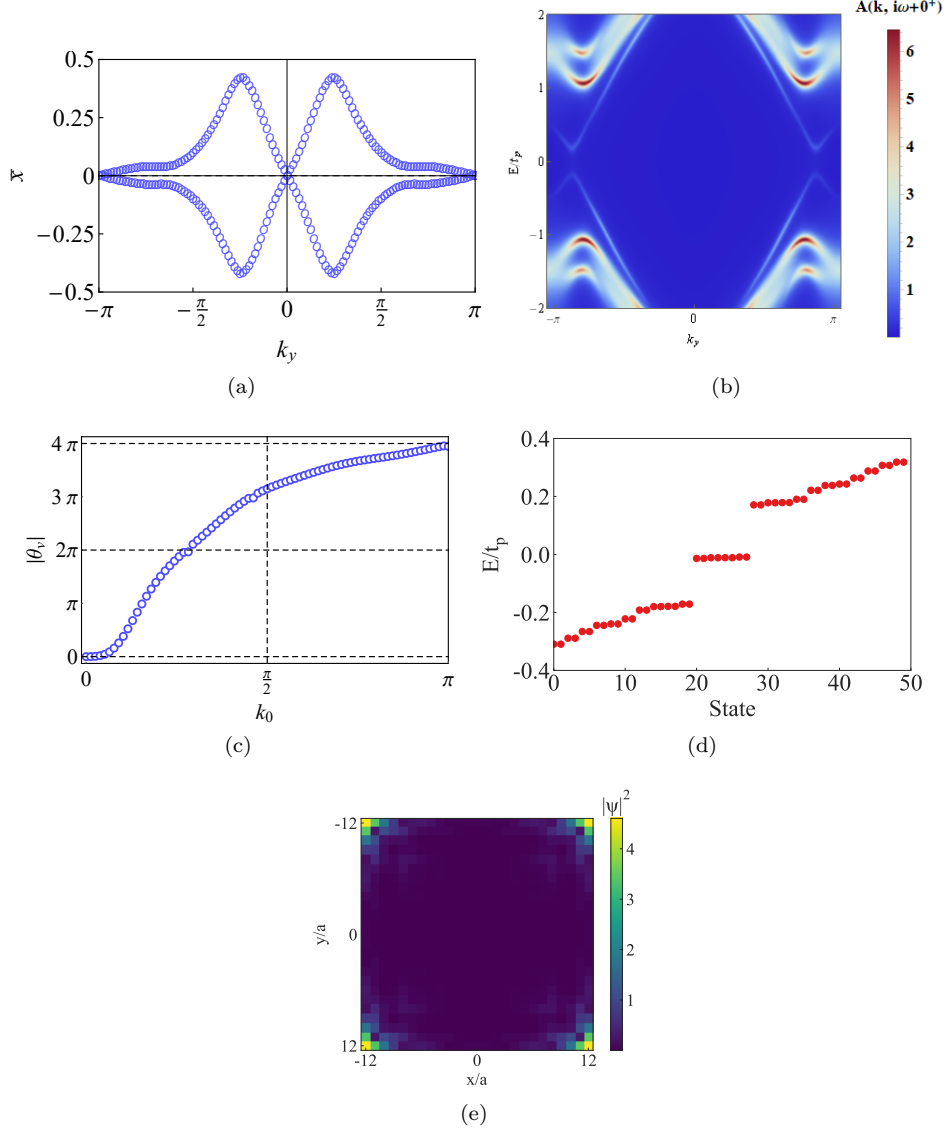


FIG. 6. (a) Wannier center charge (WCC) spectra for the tight-binding model given by eq. (A19), fixing all hopping parameters to be equal. The WCCs indicate trivial first-order topology and no gapless edge states. (b) Spectral density on (10) surface of eq. (A19), considering a semi-infinite slab geometry. The results indicate the lack of gapless edge states in accordance with the WCC spectra. (c) Results of WL calculation for eq. (A19) as a function of the area enclosed by the contour. The WL indicates a quantized non-Abelian flux of $|4\pi|$. (d) When considering a finite slab of 25 unit cells along the x and y directions, the fifty smallest magnitude states are shown. There exists eight mid-gap states at zero energy. (e) Localization of the eight mid-gap states shown in (d), indicating that these are corner localized.

dimensional topological insulators: Application to $\text{Bi}_{1-x}\text{Sb}_x$,” *Phys. Rev. B* **78**, 045426 (2008).

¹¹ Wladimir A Benalcazar, B Andrei Bernevig, and Taylor L Hughes, “Quantized electric multipole insulators,” *Science* **357**, 61–66 (2017).

¹² Frank Schindler, Ashley M. Cook, Maia G. Vergniory, Zhijun Wang, Stuart S. P. Parkin, B. Andrei Bernevig, and Titus Neupert, “Higher-order topological insulators,” *Sci. Adv.* **4** (2018), 10.1126/sci-

[adv.aat0346](#).

¹³ Mao Lin and Taylor L. Hughes, “Topological quadrupolar semimetals,” *Phys. Rev. B* **98**, 241103(R) (2018).

¹⁴ Benjamin J Wieder, Zhijun Wang, Jennifer Cano, Xi Dai, Leslie M Schoop, Barry Bradlyn, and B Andrei Bernevig, “Strong and fragile topological Dirac semimetals with higher-order Fermi arcs,” *Nat. Commun.* **11**, 1–13 (2020).

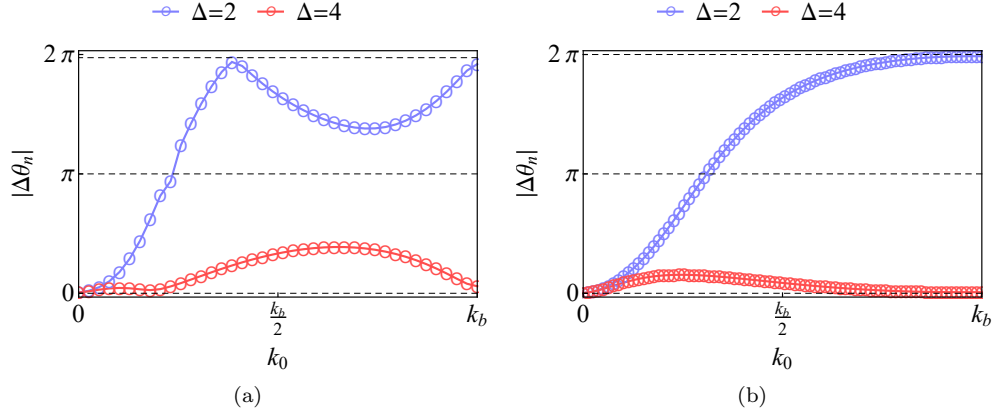


FIG. 7. (a) Results of WL calculation for C_6 symmetric model given by eq. (B1) following the path shown in Fig. (2(b)) for distinct values of the non-thermal band parameter Δ . Results demonstrate that this model supports non-Abelian flux of magnitude 2π for $\Delta = 2$, and is trivial when $\Delta = 4$. (c) Results of WL calculation for the C_3 symmetric model given by eq. (B2) for distinct values of Δ . As in the C_6 case, the results demonstrate that this model supports non-Abelian flux of magnitude 2π for $\Delta = 2$, and is trivial when $\Delta = 4$.

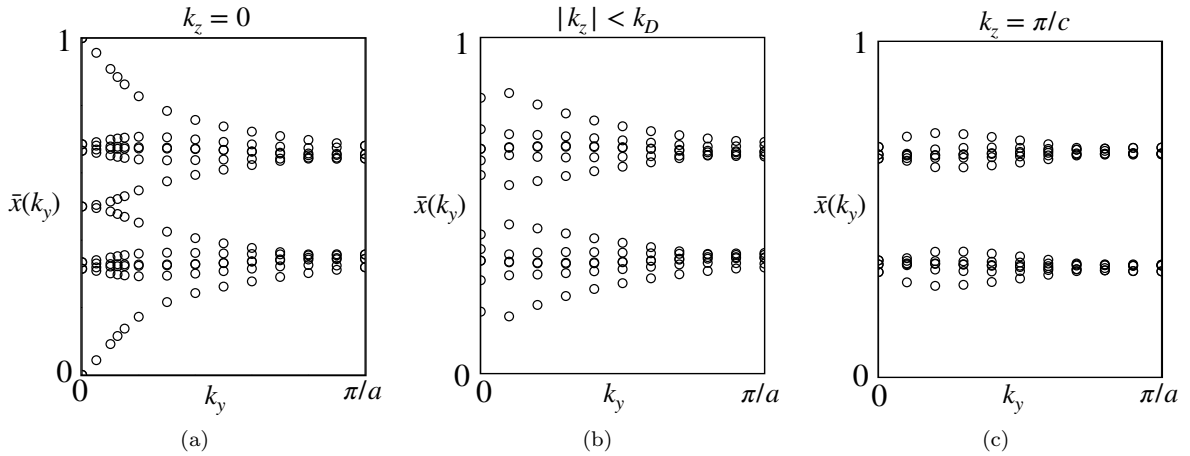


FIG. 8. The hybrid Wannier centers or spectra of Polyakov loops of non-Abelian Berry's connections of occupied bands $n = 1$ through $n = 6$ in Na_3Bi for (a) the $k_z = 0$ mirror plane, (b) the higher-order topological insulators with $|k_z| < k_D$, and (c) the topologically trivial mirror plane $k_z = \pi/c$. The gapless Wannier spectra and partner-switching allow us to identify the $k_z = 0$ plane as a first-order topological insulator with a Z_2 invariant. This is consistent with the three, occupied bands $n = 3, 5,$ and 6 supporting non-trivial, first homotopy classification, and the existence of zero-energy, helical edge states for this plane. The higher-order topological insulators and the trivial insulators exhibit gapped Wannier spectra, as none of the occupied bands support non-trivial, first homotopy classification. Therefore, the hybrid Wannier centers cannot distinguish between the trivial and the higher-order topological insulators.

¹⁵ K. G. Wilson, "Confinement of quarks," *Phys. Rev. D* **10**, 2445–2459 (1974).

¹⁶ G. 't Hooft, "A property of electric and magnetic flux in non-abelian gauge theories," *Nuc. Phys. B* **153**, 141–160 (1979).

¹⁷ M. B. Halpern, "Field-strength and dual variable formulations of gauge theory," *Phys. Rev. D* **19**, 517–530 (1979).

¹⁸ I. Y. Aref'eva, "Non-abelian stokes formula," *Theor. Math. Phys* **43**, 353–356 (1980).

¹⁹ N. E. Brali'c, "Exact computation of loop averages in two-dimensional yang-mills theory," *Phys. Rev. D* **22**, 3090–3103 (1980).

²⁰ Alexander C. Tyner, Shouvik Sur, Danilo Puggioni, James M. Rondinelli, and Pallab Goswami, "Topology of $SO(5)$ -monopoles and three-dimensional, stable Dirac semimetals," (2020), [arXiv:2012.12906](https://arxiv.org/abs/2012.12906) [cond-mat.mes-hall].

²¹ Rui Yu, Xiao Liang Qi, Andrei Bernevig, Zhong Fang, and Xi Dai, "Equivalent expression of z_2 topological

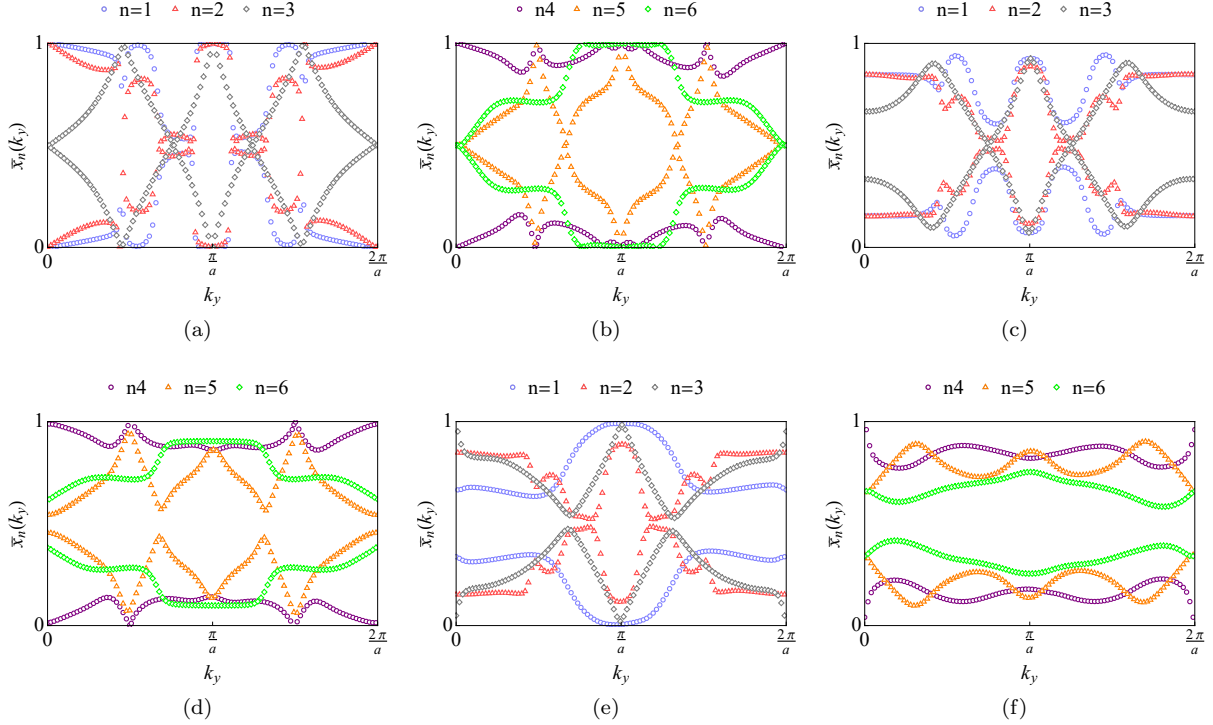


FIG. 9. The spectra of Polyakov loops (Wannier centers) of individual $SU(2)$ Berry's connections of occupied bands $n = 1$ through $n = 6$ of Na_3Bi for various planes. The Polyakov loops are computed along $M - \Gamma - M$ or \hat{x} direction and their eigenvalues can be written as $e^{\pm i\lambda_n(k_y)}$. The Wannier centers are defined as $\bar{x}_n(k_y) = \lambda_{x,n}(k_y)/(2\pi)$. (a)-(b) The Wannier spectra at $k_z = 0$ mirror plane. All non-trivial bands supporting quantized, flux at the mirror plane also exhibit gapless, Wannier spectra. The summed magnitude of mirror Chern number for occupied bands is 2π , hence, the $k_z = 0$ mirror plane is a first-order topological insulator. (c)-(d) The gapped Wannier spectra of higher-order topological insulators with $|k_z| < k_D$. (e)-(f) The gapped Wannier spectra for topologically trivial, mirror plane $k_z = \pi/c$. The trivial and higher-order topological insulators are not distinguished by the first homotopy classification of Berry's connections. They are distinguished by the second homotopy classification or the quantized, non-Abelian Berry's flux. Therefore, the reliable topological distinction among the trivial, the first-order and the higher-order topological insulators can only be made by simultaneously computing the spectra of the Polyakov loops and the Wilson loops.

- invariant for band insulators using the non-abelian berry connection," *Phys. Rev. B* **84**, 075119 (2011).
- ²² Lukasz Fidkowski, T. S. Jackson, and Israel Klich, "Model characterization of gapless edge modes of topological insulators using intermediate Brillouin-zone functions," *Phys. Rev. Lett.* **107**, 036601 (2011).
- ²³ Alexey A. Soluyanov and David Vanderbilt, "Computing topological invariants without inversion symmetry," *Phys. Rev. B* **83**, 235401 (2011).
- ²⁴ A. Alexandradinata, Xi Dai, and B. Andrei Bernevig, "Wilson-loop characterization of inversion-symmetric topological insulators," *Phys. Rev. B* **89**, 155114 (2014).
- ²⁵ Dominik Gresch, Gabriel Autès, Oleg V. Yazyev, Matthias Troyer, David Vanderbilt, B. Andrei Bernevig, and Alexey A. Soluyanov, "Z2Pack: Numerical implementation of hybrid Wannier centers for identifying topological materials," *Phys. Rev. B* **95**, 075146 (2017).
- ²⁶ Zhijun Wang, Yan Sun, Xing-Qiu Chen, Cesare Franchini, Gang Xu, Hongming Weng, Xi Dai, and Zhong Fang, "Dirac semimetal and topological phase transitions in $A_3\text{Bi}$ ($A = \text{Na}, \text{K}, \text{Rb}$)," *Phys. Rev. B* **85**, 195320 (2012).
- ²⁷ Bohm-Jung Yang and Naoto Nagaosa, "Classification of stable three-dimensional Dirac semimetals with nontrivial topology," *Nat. Commun.* **5**, 1–10 (2014).
- ²⁸ NP Armitage, EJ Mele, and Ashvin Vishwanath, "Weyl and Dirac semimetals in three-dimensional solids," *Rev. Mod. Phys.* **90**, 015001 (2018).
- ²⁹ E. V. Gorbar, V. A. Miransky, I. A. Shovkovy, and P. O. Sukhachov, "Dirac semimetals $A_3\text{Bi}$ ($a = \text{Na}, \text{K}, \text{Rb}$) as z_2 weyl semimetals," *Phys. Rev. B* **91**, 121101 (2015).
- ³⁰ Anton A. Burkov and Yong Baek Kim, " z_2 and chiral anomalies in topological Dirac semimetals," *Phys. Rev. Lett.* **117**, 136602–136606 (2016).
- ³¹ Mehdi Kargarian, Mohit Randeria, and Yuan-Ming Lu, "Are the surface fermi arcs in dirac semimetals

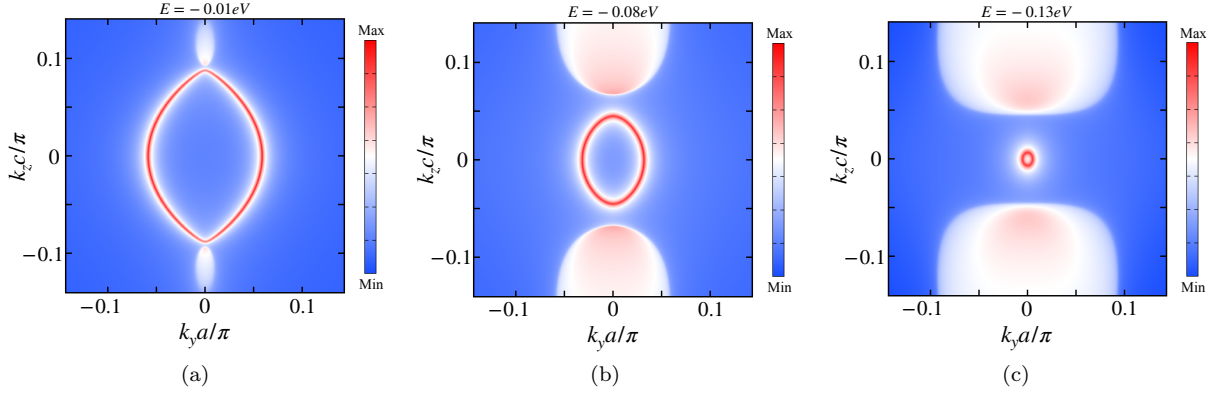


FIG. 10. The spectral intensity of surface states of Na_3Bi for different choice of reference energies. The constant energy cuts correspond to the Fermi surface of surface-bands, instead of topologically protected, loci of zero-energy states or helical Fermi arcs. Unlike the constant k_z slices, the fermiology of surface-states cannot reveal clear signatures of bulk topology.

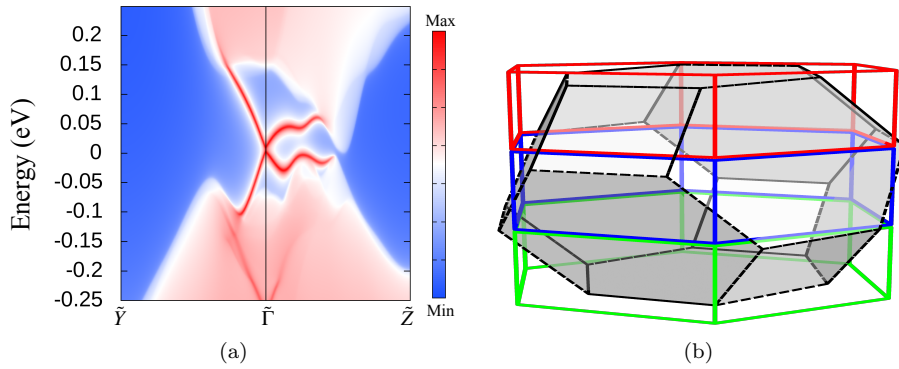


FIG. 11. (a) Spectral weight on the (100) surface of $\beta\text{-CuI}$ along high-symmetry path in the vicinity of the reference energy of the Dirac point. Surface localized states are shown to begin and terminate at the projection of the Dirac points. Calculation is shown using primitive unit cell for clarity. (b) Calculation of Wilson loop requires working in the conventional unit cell. The primitive unit cell (black outline with gray shading) is shown along with three conventional unit cells colored red, green and blue, demonstrating that the volume of the primitive unit cell is three times that of the conventional unit cell, leading to a band folding effect. For details of this band folding please consult Le et. al³³.

topologically protected?” *Proc. Natl. Acad. Sci. USA* **113**, 8648–8652 (2016).

³² Grigory Bednik, “Surface states in Dirac semimetals and topological crystalline insulators,” *Phys. Rev. B* **98**, 045140 (2018).

³³ Congcong Le, Xianxin Wu, Shengshan Qin, Yinxiang Li, Ronny Thomale, Fu-Chun Zhang, and Jiangping Hu, “Dirac semimetal in $\beta\text{-CuI}$ without surface Fermi arcs,” *Proc. Natl. Acad. Sci. USA* **115**, 8311–8315 (2018).

³⁴ Giovanni Pizzi, Valerio Vitale, Ryotaro Arita, Stefan Blugel, Frank Freimuth, Guillaume Gérañton, Marco Gibertini, Dominik Gresch, Charles Johnson, Takashi Koretsune, Julen Ibañez-Azpiroz, Hyungjun Lee, Jae-Mo Lihm, Daniel Marchand, Antimo Marrazzo, Yuriy Mokrousov, Jamal I Mustafa, Yoshiro Nohara, Yusuke Nomura, Lorenzo Paulatto, Samuel

Poncé, Thomas Ponweiser, Junfeng Qiao, Florian Thole, Stepan S Tsirkin, Małgorzata Wierzbowska, Nicola Marzari, David Vanderbilt, Ivo Souza, Arash A Mostofi, and Jonathan R Yates, “Wannier90 as a community code: new features and applications,” *J. Condens. Matter Phys.* **32**, 165902 (2020).

³⁵ MP Lopez Sancho, JM Lopez Sancho, JM Lopez Sancho, and J Rubio, “Highly convergent schemes for the calculation of bulk and surface green functions,” *J. Phys. F: Met. Phys.* **15**, 851 (1985).

³⁶ QuanSheng Wu, ShengNan Zhang, Hai-Feng Song, Matthias Troyer, and Alexey A. Soluyanov, “Wanniertools : An open-source software package for novel topological materials,” *Comput. Phys. Commun.* **224**, 405 – 416 (2018).

³⁷ Eugene Demler and Shou-Cheng Zhang, “Non-abelian holonomy of bcs and sdw quasiparticles,” *Ann. Phys.*

- 271, 83–119 (1999).
- ³⁸ Frank Wilczek and A. Zee, “Appearance of gauge structure in simple dynamical systems,” *Phys. Rev. Lett.* **52**, 2111–2114 (1984).
- ³⁹ P. M. Fishbane, S. Gasiorowicz, and P. Kraus, “Stokes’s theorems for non-abelian fields,” *Phys. Rev. D* **24**, 2324–2329 (1981).
- ⁴⁰ D. I. Diakonov and V. Yu. Petrov, “A formula for the Wilson loop,” *Phys. Lett. B* **224**, 131–135 (1989).
- ⁴¹ R. Matsudo and K.-I. Kondo, “Non-Abelian Stokes theorem for the Wilson loop operator in an arbitrary representation and its implication to quark confinement,” *Phys. Rev. D* **92**, 125038 (2015).
- ⁴² G. Kresse and J. Furthmüller, “Efficient iterative schemes for ab initio total-energy calculations using a plane-wave basis set,” *Phys. Rev. B* **54**, 11169–11186 (1996).
- ⁴³ G. Kresse and D. Joubert, “From ultrasoft pseudopotentials to the projector augmented-wave method,” *Phys. Rev. B* **59**, 1758–1775 (1999).
- ⁴⁴ John P. Perdew, Kieron Burke, and Matthias Ernzerhof, “Generalized gradient approximation made simple,” *Phys. Rev. Lett.* **77**, 3865–3868 (1996).
- ⁴⁵ Z. K. Liu, B. Zhou, Y. Zhang, Z. J. Wang, H. M. Weng, D. Prabhakaran, S.-K. Mo, Z. X. Shen, Z. Fang, X. Dai, Z. Hussain, and Y. L. Chen, “Discovery of a three-dimensional topological Dirac semimetal Na₃Bi,” *Science* **343**, 864–867 (2014).
- ⁴⁶ Su-Yang Xu, Chang Liu, Satya K. Kushwaha, Raman Sankar, Jason W. Krizan, Ilya Belopolski, Madhab Neupane, Guang Bian, Nasser Alidoust, Tay-Rong Chang, Horng-Tay Jeng, Cheng-Yi Huang, Wei-Feng Tsai, Hsin Lin, Pavel P. Shibayev, Fang-Cheng Chou, Robert J. Cava, and M. Zahid Hasan, “Observation of Fermi arc surface states in a topological metal,” *Science* **347**, 294–298 (2015).
- ⁴⁷ Satya K Kushwaha, Jason W Krizan, Benjamin E Feldman, Andras Gyenis, Mallika T Randeria, Jun Xiong, Su-Yang Xu, Nasser Alidoust, Ilya Belopolski, Tian Liang, *et al.*, “Bulk crystal growth and electronic characterization of the 3D Dirac semimetal Na₃Bi,” *APL Mater.* **3**, 041504 (2015).
- ⁴⁸ Jun Xiong, Satya K Kushwaha, Tian Liang, Jason W Krizan, Max Hirschberger, Wudi Wang, Robert Joseph Cava, and Nai Phuan Ong, “Evidence for the chiral anomaly in the Dirac semimetal Na₃Bi,” *Science* **350**, 413–416 (2015).
- ⁴⁹ Aiji Liang, Chaoyu Chen, Zhijun Wang, Youguo Shi, Ya Feng, Hemian Yi, Zhuojin Xie, Shaolong He, Junfeng He, Yingying Peng, Yan Liu, Defa Liu, Cheng Hu, Lin Zhao, Guodong Liu, Xiaoli Dong, Jun Zhang, M Nakatake, H Iwasawa, K Shimada, M Arita, H Namatame, M Taniguchi, Zuyan Xu, Chuangtian Chen, Hongming Weng, Xi Dai, Zhong Fang, and Xing-Jiang Zhou, “Electronic structure, Dirac points and Fermi arc surface states in three-dimensional Dirac semimetal Na₃Bi from angle-resolved photoemission spectroscopy,” *Chinese Phys. B* **25**, 077101 (2016).
- ⁵⁰ Eslam Khalaf, Hoi Chun Po, Ashvin Vishwanath, and Haruki Watanabe, “Symmetry indicators and anomalous surface states of topological crystalline insulators,” *Phys. Rev. X* **8**, 031070 (2018).
- ⁵¹ Jorrit Kruthoff, Jan de Boer, Jasper van Wezel, Charles L. Kane, and Robert-Jan Slager, “Topological classification of crystalline insulators through band structure combinatorics,” *Phys. Rev. X* **7**, 041069 (2017).
- ⁵² Barry Bradlyn, L Elcoro, Jennifer Cano, MG Vergniory, Zhijun Wang, C Felser, MI Aroyo, and B Andrei Bernevig, “Topological quantum chemistry,” *Nature* **547**, 298–305 (2017).
- ⁵³ Hoi Chun Po, Ashvin Vishwanath, and Haruki Watanabe, “Symmetry-based indicators of band topology in the 230 space groups,” *Nat. Commun.* **8**, 1–9 (2017).
- ⁵⁴ Jennifer Cano, Barry Bradlyn, Zhijun Wang, L. Elcoro, M. G. Vergniory, C. Felser, M. I. Aroyo, and B. Andrei Bernevig, “Building blocks of topological quantum chemistry: Elementary band representations,” *Phys. Rev. B* **97**, 035139 (2018).
- ⁵⁵ MG Vergniory, L Elcoro, Claudia Felser, Nicolas Regnault, B Andrei Bernevig, and Zhijun Wang, “A complete catalogue of high-quality topological materials,” *Nature* **566**, 480–485 (2019).
- ⁵⁶ Tiantian Zhang, Yi Jiang, Zhida Song, He Huang, Yuqing He, Zhong Fang, Hongming Weng, and Chen Fang, “Catalogue of topological electronic materials,” *Nature* **566**, 475–479 (2019).
- ⁵⁷ Feng Tang, Hoi Chun Po, Ashvin Vishwanath, and Xiangang Wan, “Efficient topological materials discovery using symmetry indicators,” *Nat. Phys.* **15**, 470–476 (2019).
- ⁵⁸ Feng Tang, Hoi Chun Po, Ashvin Vishwanath, and Xiangang Wan, “Comprehensive search for topological materials using symmetry indicators,” *Nature* **566**, 486–489 (2019).
- ⁵⁹ Maia G Vergniory, Benjamin J Wieder, Luis Elcoro, Stuart SP Parkin, Claudia Felser, B Andrei Bernevig, and Nicolas Regnault, “All topological bands of all stoichiometric materials,” arXiv:2105.09954 (2021).
- ⁶⁰ Yuanfeng Xu, Luis Elcoro, Zhi-Da Song, Benjamin J Wieder, MG Vergniory, Nicolas Regnault, Yulin Chen, Claudia Felser, and B Andrei Bernevig, “High-throughput calculations of magnetic topological materials,” *Nature* **586**, 702–707 (2020).
- ⁶¹ Luis Elcoro, Benjamin J Wieder, Zhida Song, Yuanfeng Xu, Barry Bradlyn, and B Andrei Bernevig, “Magnetic topological quantum chemistry,” arXiv:2010.00598 (2020).
- ⁶² Adrien Bouhon, Gunnar F. Lange, and Robert-Jan Slager, “Topological correspondence between magnetic space group representations and subdimensions,” *Phys. Rev. B* **103**, 245127 (2021).
- ⁶³ Gunnar F. Lange, Adrien Bouhon, and Robert-Jan Slager, “Subdimensional topologies, indicators, and higher order boundary effects,” *Phys. Rev. B* **103**, 195145 (2021).
- ⁶⁴ Zhijun Wang, Hongming Weng, Quansheng Wu, Xi Dai, and Zhong Fang, “Three-dimensional dirac semimetal and quantum transport in cd₃as₂,” *Phys. Rev. B* **88**, 125427 (2013).

- ⁶⁵ Q. D. Gibson, L. M. Schoop, L. Muechler, L. S. Xie, M. Hirschberger, N. P. Ong, R. Car, and R. J. Cava, “Three-dimensional Dirac semimetals: Design principles and predictions of new materials,” *Phys. Rev. B* **91**, 205128 (2015).
- ⁶⁶ Rui Yu, Hongming Weng, Zhong Fang, Xi Dai, and Xiao Hu, “Topological node-line semimetal and Dirac semimetal state in antiperovskite Cu_3PdN ,” *Phys. Rev. Lett.* **115**, 036807 (2015).
- ⁶⁷ Yongping Du, Bo Wan, Di Wang, Li Sheng, Chungang Duan, and Xiangang Wan, “Dirac and Weyl semimetal in $XY\text{Bi}$ ($X = \text{Ba, Eu}$; $Y = \text{Cu, Ag}$ and Au),” *Sci. Rep.* **5**, 14423 (2015).
- ⁶⁸ Huaqing Huang, Shuyun Zhou, and Wenhui Duan, “Type-II Dirac fermions in the PtSe_2 class of transition metal dichalcogenides,” *Phys. Rev. B* **94**, 121117 (2016).
- ⁶⁹ Rokyeon Kim, Bohm-Jung Yang, and Choong H Kim, “Crystalline topological Dirac semimetal phase in rutile structure β' - PtO_2 ,” *Phys. Rev. B* **99**, 045130 (2019).
- ⁷⁰ Tay-Rong Chang, Su-Yang Xu, Daniel S. Sanchez, Wei-Feng Tsai, Shin-Ming Huang, Guoqing Chang, Chuang-Han Hsu, Guang Bian, Ilya Belopolski, Zhi-Ming Yu, Shengyuan A. Yang, Titus Neupert, Horng-Tay Jeng, Hsin Lin, and M. Zahid Hasan, “Type-II symmetry-protected topological Dirac semimetals,” *Phys. Rev. Lett.* **119**, 026404 (2017).
- ⁷¹ Congcong Le, Shengshan Qin, Xianxin Wu, Xia Dai, Peiyuan Fu, Chen Fang, and Jiangping Hu, “Three-dimensional topological critical Dirac semimetal in $a\text{MgBi}$ ($a = \text{k, rb, cs}$),” *Phys. Rev. B* **96**, 115121 (2017).
- ⁷² Zhiyong Lin, Chongze Wang, Pengdong Wang, Seho Yi, Lin Li, Qiang Zhang, Yifan Wang, Zhongyi Wang, Hao Huang, Yan Sun, Yaobo Huang, Dawei Shen, Donglai Feng, Zhe Sun, Jun-Hyung Cho, Changgan Zeng, and Zhenyu Zhang, “Dirac fermions in antiferromagnetic fcsn kagome lattices with combined space inversion and time-reversal symmetry,” *Phys. Rev. B* **102**, 155103 (2020).